Supplementary information

On-chip droplet analysis and cell spheroid screening by capillary wrapping enabled shape-adaptive ferrofluid transporters

Xuejiao Wang[a], Xin Li[a], Aoyang Pu[a], Ho Bak Shun[a], Cien Chen[a], Liqing Ai[a], Zhaoling Tan[a], Jilin Zhang[a], Kai Liu[a], Jun Gao*[b], Kiwon Ban*[a], Xi Yao*[a,c]

[a]Department of Biomedical Sciences, Department of Infectious Diseases and Public Health, City University of Hong Kong, Tat Chee Avenue, Kowloon Tong, Hong Kong, P. R. China;

[b]Qingdao Institute of Bioenergy and Bioprocess Technology, Chinese Academy of Sciences, Qingdao 266101, Shandong province, P. R. China;

[c]Shenzhen Research Institute, City University of Hong Kong, Shenzhen 518075 P. R. China

*To whom correspondence may be addressed. E-mail: xi.yao@cityu.edu.hk or Ban.KW@cityu.edu.hk or jun.gao@qibebt.ac.cn.

Supporting Information Text

Note S1. The process of wrapping.

The densities of water (0.998 kg/m^3) and ferrofluid (1.827 kg/m^3) are higher than that of the silicone oil (0.944 Kg/m^3), so their gravities overperform the buoyance exerted by the silicone oil. Therefore, the droplets sink onto the surface of polystyrene (Fig. S1). The calculated Weber number (We= $\frac{\rho v^2 l}{\gamma}$, where ρ is the density of the droplet, v is the velocity, l is the droplet diameter, and γ is the surface tension of the droplet) is as less as ~10^{-5} in the system, indicating that surface tension governs the process. When the fluorinated ferrofluid contacts the droplet, it will spread on the interface of the droplet and the silicone oil. This wetting phenomenon is explained by the analysis of the spreading parameter *S*:[1]

$$S = \gamma_{d-oil} - (\gamma_{d-f} + \gamma_{f-oil}) \quad (1)$$

where γ_{d-oil}=41.33 mN/m, γ_{d-f}=19.29 mN/m, γ_{f-oil}=16.47 mN/m are the interfacial tensions at droplet/oil, droplet/ferrofluid, and ferrofluid/oil interfaces respectively. Substituting the relative values into equation (1), we get S>0. The ferrofluid will spontaneously spread on the surface of the water droplet, which is so-called wrapping process.

KSV Instruments (CAM 101 system) was used to capture drop of various liquids at mechanical equilibrium. The surface tension was measured through the Pendant drop method.

Note S2. The process of actuation.

Droplet actuation conducted by transporter is relatively modest, considering a low Reynolds number ($Re = \frac{\rho v l}{\eta}$, where ρ is the density of the droplet, v is the velocity, l is the droplet diameter, and η is the dynamic viscosity of the droplet) as less as 0.1. The elastic force arising from the droplet deformation was ignored since the deformation transiently occurs only when approaching the magnetic field center (Fig. 1C). We rationalized the actuation process with a simplified model. The wrapped is regarded as a whole with a diameter of *D*. During movement, the droplet is mainly subject to a magnetic force and a drag force. The magnetic force is exerted from an external magnetic field, which can be described as:

$$F_{mag,x} = M\frac{dB_x}{dx} \quad (2)$$

where B_x is the magnetic flux density in the x direction driving the droplet, and M is the magnetization of the ferrofluid, determined as $M = V_w \chi \frac{B_0}{\mu}$. χ is the susceptibility of the ferrofluid, B_0 is the magnetic flux density of the magnet, and μ is the magnetic permeability of the ferrofluid (~$4\pi \times 10^{-7}$ N A^{-2}).

The resultant force of the movement resistance is given by: $F_{drag} = F_f + F_h$, as depicted in Fig. S5. F_h derivates from the contact angle hysteresis. And F_f is the interfacial friction.

Once the magnetic force overcomes the movement resistance, the droplet transportation will be initiated. During transportation, except for the dynamic friction resistance and contact angle hysteresis, the droplet will experience the viscous drag force from the silicone oil. Because the low interfacial friction and a minimum contact area between the wrapped droplet and the substrate, the frictional force F_f and the influence of F_h during movement are negligible. Thus, the viscous drag force dominates the resistance during movement: $F_{drag} = F_v$. According to the Hadamard-Rybczynski equation, the viscous drag force for droplet under oil can be described as[2]:

$$F_v = 3\pi D\eta v \frac{1 - 2\eta/3\eta_{fd}}{1 + \eta/\eta_{fd}} \quad (3)$$

where η is the dynamic viscosity of the silicone oil, η_{fd} is the dynamic viscosity of the ferrofluid-wrapped droplet, v is the moving velocity of the ferrofluid-wrapped droplet. When the η is far less than η_{fd}, the spherical droplet can be considered as a rigid body. In this case, formula (3) can be written as:

$$F_v = 3\pi D\eta v. \quad (4)$$

The force balance can be described as an equation of the barycenter position x:

$$M\frac{dB_x}{dx} - 3\pi D\eta\frac{dx}{dt} - m_{w+d}\frac{d^2x}{dt^2} = 0 \quad (5)$$

where m_{w+d} is the mass of transporter (w) and droplet (d). (5) can be further described as:

$$\frac{dv}{dt}+\frac{3\pi D\eta}{m_{d+w}}v-\frac{M\frac{dB_x}{dx}}{m_{d+w}}=0 \quad (6)$$

Assuming a constant gradient magnetic field, formula (6) is:

$$v=\frac{\beta}{\alpha}(1-exp(-\alpha t)) \quad (7)$$

with $\alpha=\frac{3\pi D\eta}{m_{d+w}}$ and $\beta=\frac{M\frac{dB_x}{dx}}{m_{d+w}}$.

And the average velocity can be calculated as:

$$\bar{v}=\frac{\int_0^t v d_t}{t}=\frac{\beta}{\alpha}+\frac{\beta}{\alpha^2 t}(e^{-\alpha t}-1) \quad (8)$$

Note S3. The analysis of droplet transportation.

The actual magnetic field boundary conditions are difficult to give, so the theoretical average velocity cannot be directly calculated from formula (8). But we can analyze the conditions that affect the transportation speed and verify them through experiments. When using the same droplet size to study the influence of magnetic field in silicone oil with fixed viscosity, the D, m_{w+d}, and η is fixed. Therefore, α can be considered as a constant. In this case, the formula (8) can be further written as: $\bar{v}=\beta(\frac{1}{\alpha}+\frac{1}{\alpha^2 t}(e^{-\alpha t}-1))$. Only the magnetic flux density (B_0) is the variable. So, the average velocity $\bar{v}$ should be a directly proportional function of B_0 in theory. As shown in Figure 2B, the average velocity increases with B_0. When fitting the tested data in Figure 2B, the equation is $\bar{v}=1.5+5.3\times B_0$ mm/s, $\bar{v}=-0.4+3.6\times B_0$ mm/s, and $\bar{v}=-2+3.0\times B_0$ mm/s for 1 μL, 5 μL, and 10 μL droplet respectively. The fitted curves indicate the average velocity is a linear function of magnetic flux density, which is consistent with the trend of theoretical analysis. However, the equations are not directly proportional function. This could be caused by that the change of magnets lead to changed $\frac{dB_x}{dx}$. The

deformation of magnetic fluid under a non-uniform magnetic field is nonlinear, which leads to changes in the contact area between the entire droplet and the substrate during movement, thereby affecting the friction force experienced by the droplet. Moreover, the movement of droplets is a process of acceleration and deceleration, and the viscosity force received during the process actually changes in real time. Additionally, the average velocity for a droplet (1 μL) increased with larger volume of ferrofluid transporter (Fig. S8). This is because the positive correlation between the M and ferrofluid volume resulted to an increased magnetic force. In this case, the increased magnetic force overweighted the change of the drag force.

When using the same droplet size and magnet (1 mT, 2 mT, 3 mT) to study the influence of silicone oil, the D, m_{w+d}, M and $\frac{dB_x}{dx}$ are fixed and β can be considered as constant. The variable is the η of the silicone oil. And the formula (8) can be written as: $\bar{v} \sim \frac{\beta}{\alpha} + \frac{\beta}{\alpha^2 t}\left(e^{-\alpha t} - 1\right)$. Because the viscosity of the silicone oil ranges from 10 to 100 mPa·s, the wrapped droplet size D is ~1 mm, and m_{w+d} is ~2.8 g, the $\frac{1}{\alpha^2 t}\left(e^{-\alpha t} - 1\right)$ is rather small so it can be ignored. Thus, the average velocity as a function of oil viscosity can be further simplified as: $\bar{v} \sim \frac{1}{\alpha}$. As shown in Figure 2C, the average velocity decreased with increasing viscosity of silicone oil. The fitted curves are $\bar{v} = 15.75 \times \frac{1}{\eta^{0.63}}$ mm/s, $\bar{v} = 107.77 \times \frac{1}{\eta^{0.74}}$ mm/s, and $\bar{v} = 327.34 \times \frac{1}{\eta^{0.93}}$ mm/s for droplets transportation under magnetic flux density of 1 mT, 2 mT, 3 mT, which is consistent with the trend of theoretical analysis.

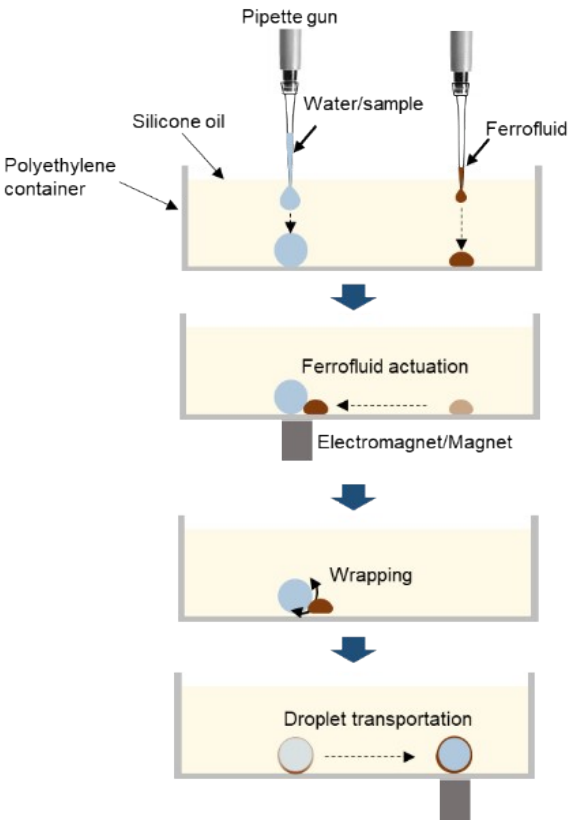

Figure S1. Demonstration of the transporter system. The platform consists of a transparent polystyrene container filled with silicone oil. The droplets and ferrofluid transporter were added to the polystyrene container through a pipette unless further emphasized. Due to the influence of gravity, the droplets and ferrofluid transporter sink to the bottom of the container. The ferrofluid responds to an external magnetic field generated by a magnet or electromagnet and be guided to contact the droplet. Once the ferrofluid contact with the droplet, the ferrofluid spontaneously wraps the droplet. Upon an external magnetic field applied in the system, the transporter can transport the droplet towards the magnetic field center.

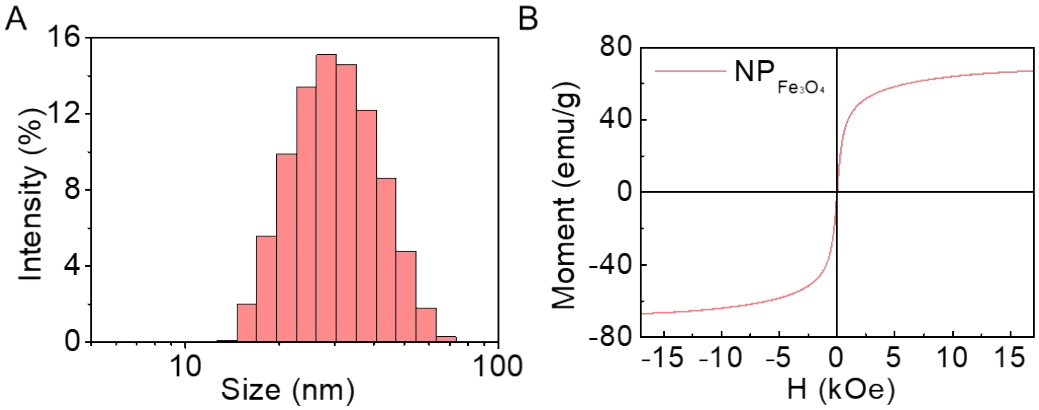

Fig. S2. The properties of the ferrofluid. (A) The particle size distribution of the dispersed Fe_3O_4 nanoparticles ($NP_{Fe_3O_4}$) in fluorinated oil. The average diameter was measured to be 32 nm. (B) The magnetization curve of the modified nanoparticles before dilution.

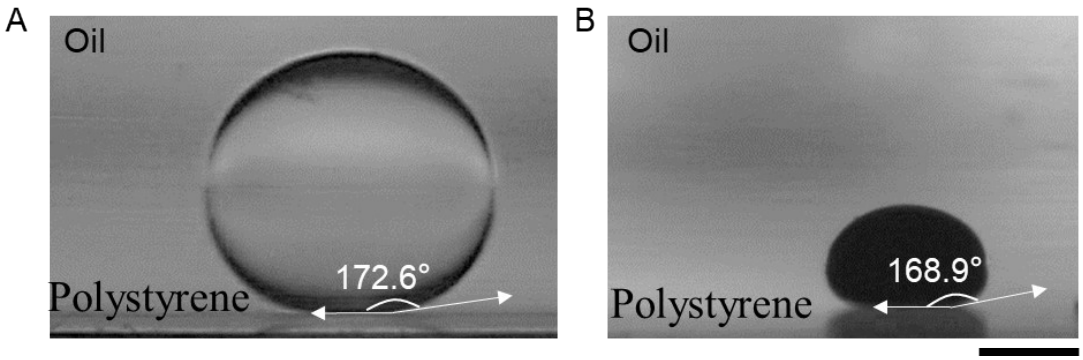

Fig. S3. The water droplet (A) and ferrofluid droplet (B) both show spherical shapes on oil-submerged polystyrene with a contact angle of 172.6° and 168.9° respectively. The volume of the water droplet is 10 μL and of fluorinated ferrofluid is 1 μL. The scale bar is 1 mm.

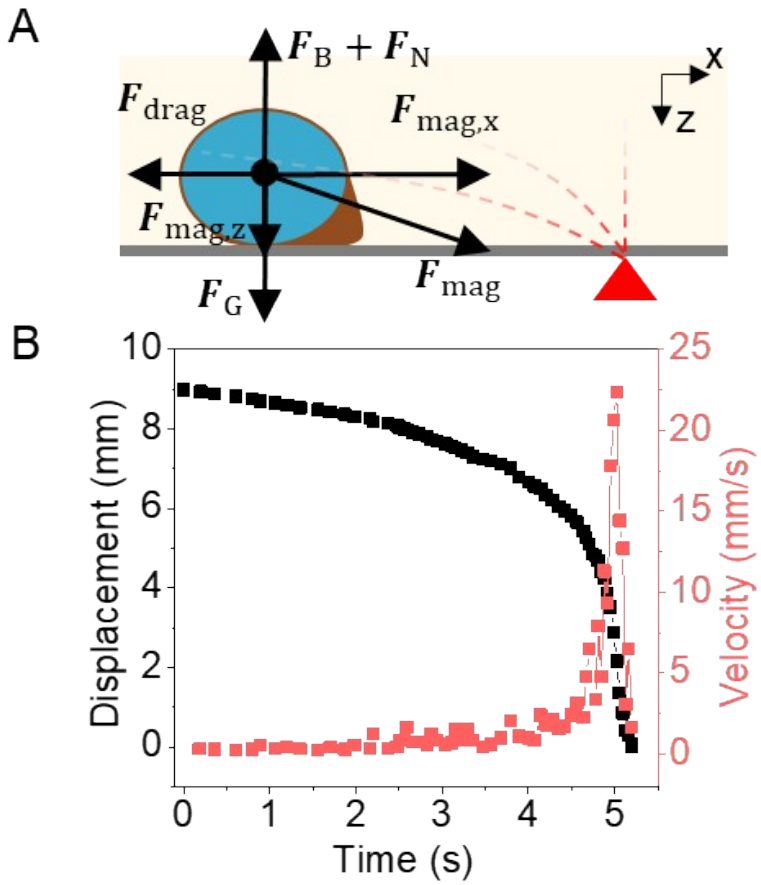

Fig. S4. The analysis of droplet behavior during movement. (A) Schematic illustration of force analysis. (B) The measured droplet displacement and calculated velocity of the droplet transportation in Fig. 1C. At the initial stage, the magnetic force acting onto the droplet increased gradually and so that the velocity of the droplet accelerated with respect to time. The velocity reached a maximum value when the magnetic field in x direction reached the maximum. Approaching the magnetic field center, the velocity of the droplet undergoes a rapid retardation which originates from a plummeted magnetic force in the x direction and increased pinning force in the z direction. At the magnetic field center, the magnetic force in the z direction reached the maximum value, whereas the force is balanced in x direction, which explains that the droplet can be precisely positioned by the external magnetic field (Fig. 1C).

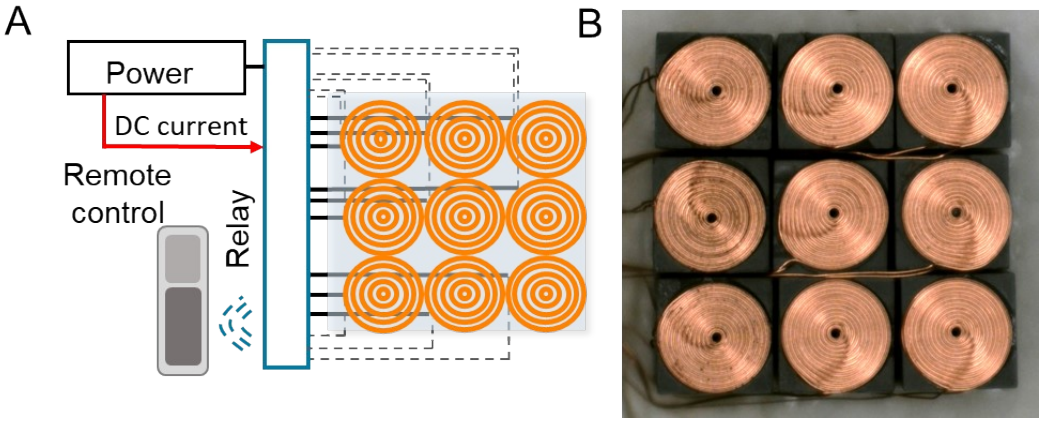

Fig. S5. (A) Schematic of the electromagnetic control system for programmable control. (B) Photo image of a 3×3 electromagnetic coil array for programmable control. A vertical magnetic field is generated using DC power supply because of Ampère's circuital law, which lift the magnet inside the contain up for enhancing on-site magnetic field. The magnet will be released once the power is off. This power on-and-off caused lifting up-and-down mode was used for magnetic field strength regulation. The hight of the magnet from the coil was set as 7 mm.

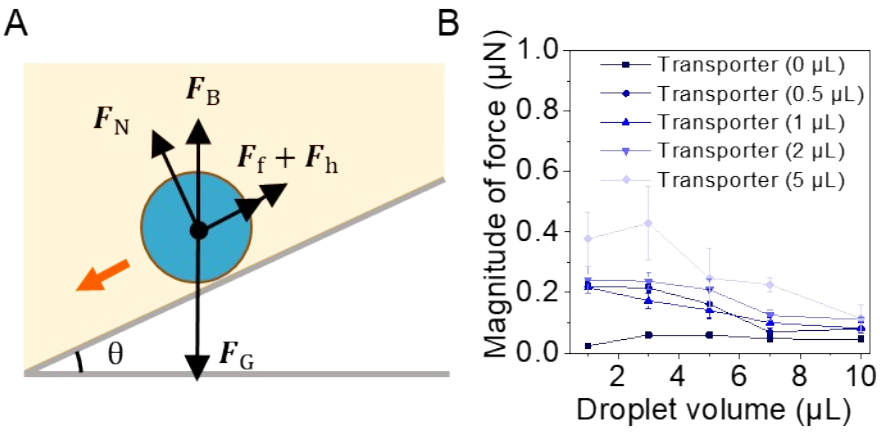

Fig. S6. The force analysis of the movement resistance. (A) Schematic diagram of the force analysis. By tilting the container, the minimum sliding angle was examined for different droplets. Under critical conditions, the balanced force in the direction of the slope can be described as: $(F_G - F_B)cos\theta = F_f + F_h$, where F_G is the gravity of the wrapped droplet, F_B is the buoyancy of wrapped droplet in silicone oil, F_f is the interfacial friction of wrapped droplet respectively. F_h arises from the contact angle hysteresis. (B) The calculated magnitude of force (referring to movement resistance $F_{drag} = F_f + F_h$ of different droplets, which is in a range of 0.1~0.5 mN. Therefore, it is easy for transporter to actuate the droplet.

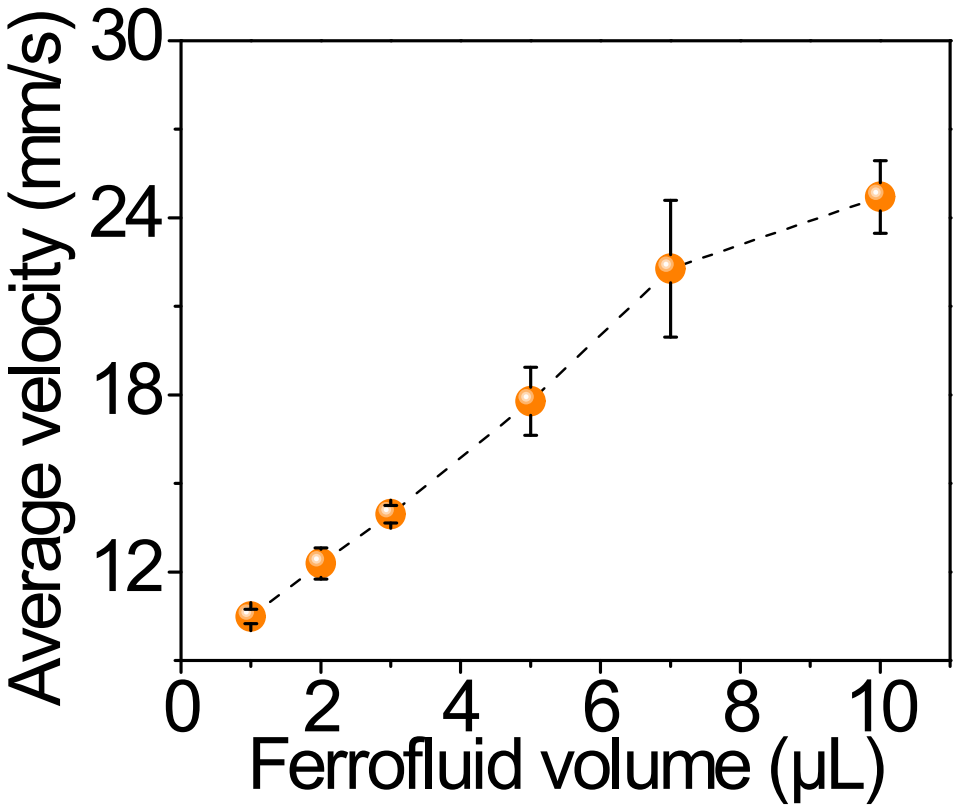

Fig. S7. Average velocity of the actuation of droplet (1 μL) vs. the ferrofluid volume, under the same magnetic field (~1 mT) and moving distance (10 mm).

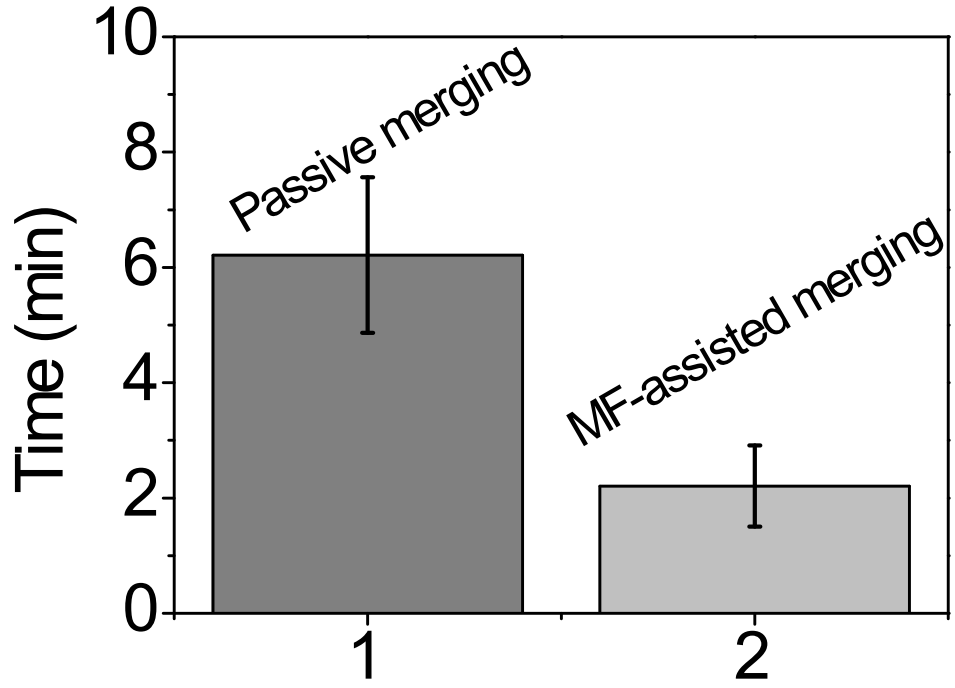

Fig. S8. Comparison for droplet merging time with passive and magnetic field (OF) assistance. Two droplets with the volume of 5 μL were first actuated to contact by ferrofluid transporter. The time after droplet contact and at droplet merge were recorded.

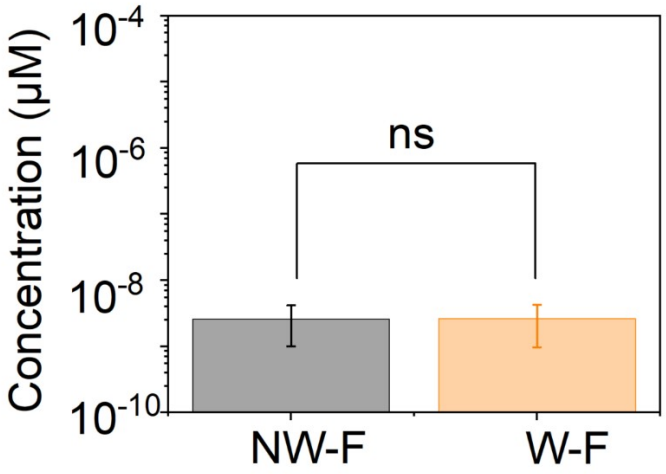

Figure S9. Characterization of diffusion into the silicone oil. Rhodamine 6G (R6G) was used to characterize the diffusion. 10 μL R6G with a concentration of 100 μM was injected to a polystyrene container filled with 10 mL silicone oil. After 24 hours incubation, 300 μL of silicone oil was transferred to a plate reader for fluorescence measurement (480 nm excitation/500 nm emission, Synergy HT, BioTek Instruments, Inc., USA). NW-F and W-F represent droplet was not wrapped by ferrofluid and wrapped by ferrofluid respectively. All values represent the mean ± SD for n = 3 independent experiments.

Figure S10. A 10 μL water droplet was successfully transported on a tilted surface (8°) by 1 μL transporter. The scale bar is 2 mm.

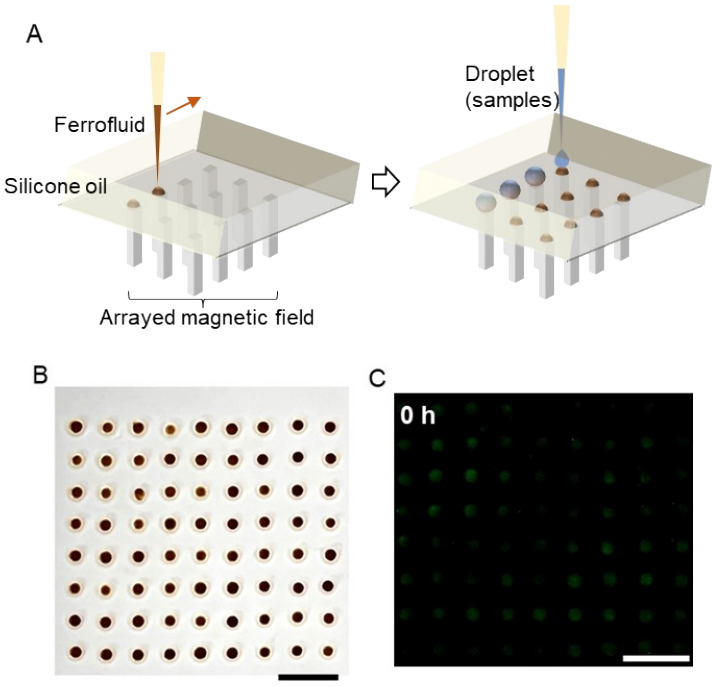

Fig. S11. The fabrication of transporter manipulated droplet array. (A) Schematic diagram of fabricating transporter-manipulated droplet array. Under the guidance of an arrayed magnetic field, transporters were precisely positioned on each magnetic field center for droplet wrapping, thereby establishing the droplet array. (B) Optical image of an 8×9 droplet array. The total volume of ferrofluid was 10 μL and each water droplet has a volume of 1 μL. (C) Fluorescent image of the droplet (containing *E. Coli*) array. The scale bar is 5 mm.

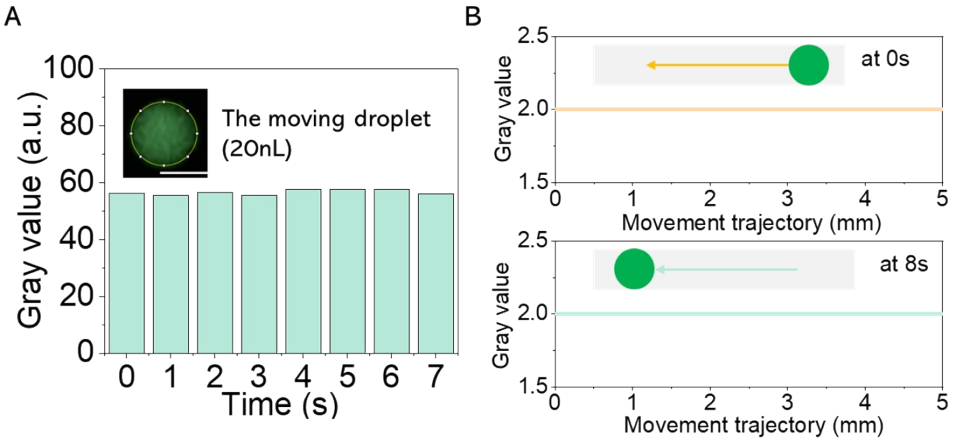

Figure S12. (A) The fluorescent intensity of the moving droplet (20 nL) in Figure 4C. The signal of the droplet remains unchanged during transportation. The scale bar is 0.3mm. (B) The fluorescent intensity along the droplet movement trajectory before movement (at 0s) and after the droplet was removed (at 8s). No fluorescent signal was observed on the droplet movement trajectory. The results indicate that there was no fouling trace when manipulating droplets on the chip.

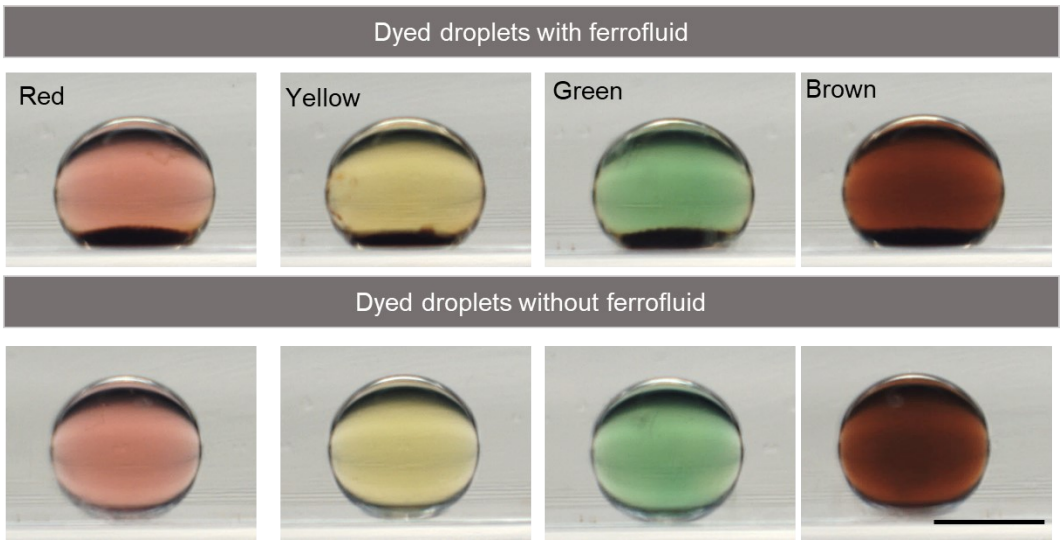

Fig. S13. Optical photographs show the side view of dyed droplets (10 μL) with and without ferrofluid transporter (1 μL). The magnetic field was on to immobilize the droplet, and the ferrofluid was therefore accumulated to the bottom of the droplets. Food dyes including carmine (red), tartrazine (yellow), fruit-green, and carmine mixed fruit-green (brown) were used (5 mg dye/10 mL water) for coloration. The scale bar is 2 mm.

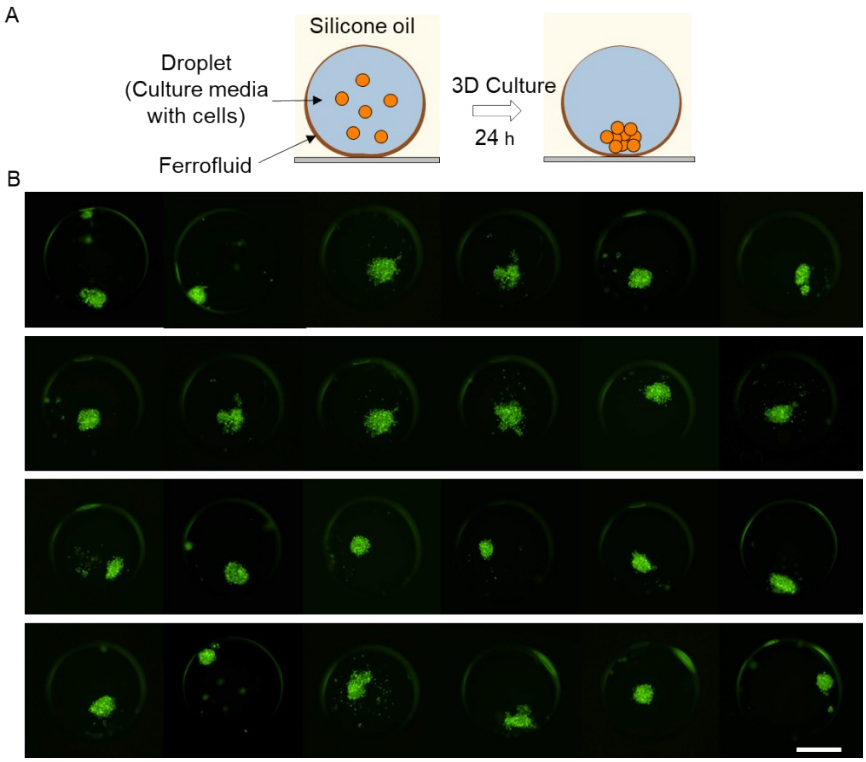

Fig. S14. (A) Illustration of cells forming spheroid inside droplet after 24 hours of culturing. (B) Images of 24 droplets containing HFDPC after 24 h incubation. Cells in each droplet all formed a 3D aggregates. The scale bar is 500 μm.

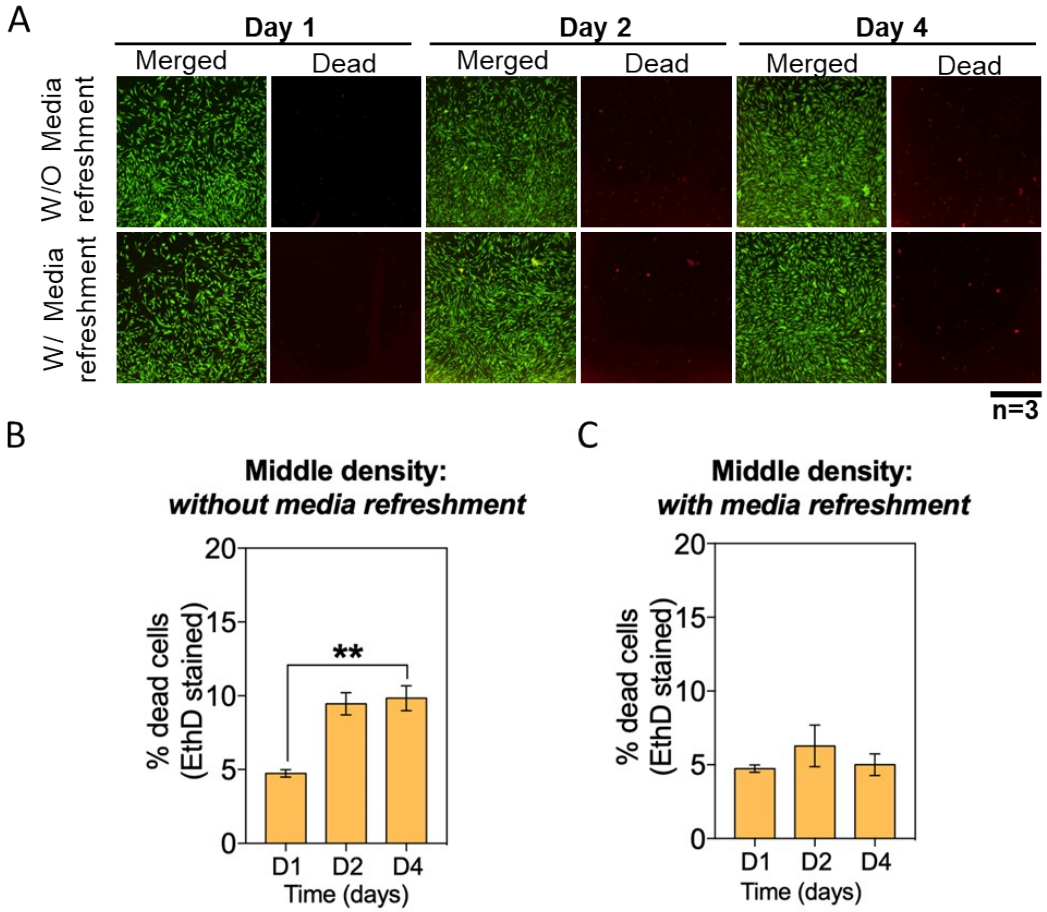

Fig. S15. Cell viability in 2D monolayer culturing. (A) Fluorescent images of cell incubation at day 1, 2 and 4 without and with (every 24 hours) media refreshment. The quantification of the percentage of Dead cells without (B) and with (C) media refreshment. Compared with aggregated cells in a ferrofluid transport manipulation chip (Figure 4B and 4C), unaggregated cells in 2D culture are more likely to die, especially in the absence of medium renewal. The scale bar is 200 μm.

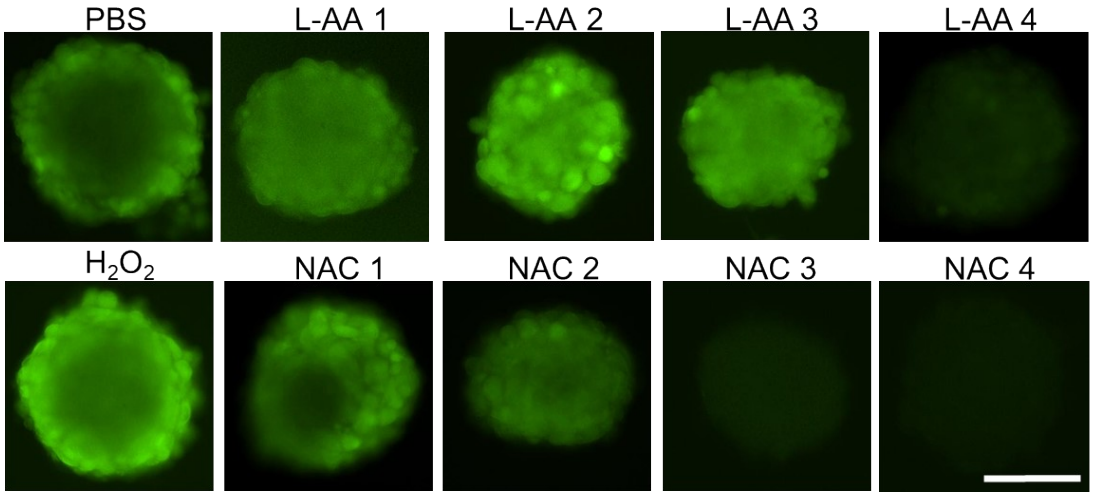

Fig. S16. Determination of intracellular ROS levels in H_2O_2-treated human HFDPC aggregates by DCFDA staining. L-AA 1-4 represents 10, 100, 150, and 200 μM of L-AA respectively. NAC 1-4 represents 4, 20, 30, and 40 mM of L-AA respectively. The scale bar is 100 μm.

Movie S1 The droplet wrapping process of ferrofluid transporter. The ferrofluid transporter was guided to the droplet under external magnetic field and proceeds wrapping spontaneously after contact with the droplet.

Movie S2 The transportation of droplet by ferrofluid transporter under a magnetic field gradient.

Movie S3 Programmed digital actuation of the droplet by ferrofluid transporter.

Movie S4 Selective actuation of droplets. Droplet positioning and actuation can be on-demand controlled by turning the strength of the magnetic field.

Movie S5 Programmed droplet gating and sorting by ferrofluid transporter. A droplet can be controlled to travel across two droplets or chosen to merge with one droplet.

Movie S6 Target droplet delivery in droplet array on transporter manipulated chip.

Movie S7 Droplet replacement on ferrofluid transporter manipulated chip.

Movie S8 Parallel tests of ferrofluid transporter conducted sample preparation for PCR.

SI References

1. D. Bonn, J. Eggers, J. Indekeu, J. Meunier and E. Rolley, *Reviews of Modern Physics*, 2009, **81**, 739-805.
2. F. M. White, 1991.